UC Berkeley
UC Berkeley Previously Published Works

Title

Large regional shortwave forcing by anthropogenic methane informed by Jovian observations

Permalink

https://escholarship.org/uc/item/4gb2d24h

Journal

Science Advances, 4(9)

ISSN

2375-2548

Authors

Collins, William D
Feldman, Daniel R
Kuo, Chaincy
et al.

Publication Date

2018-09-07

DOI

10.1126/sciadv.aas9593

Peer reviewed

Large regional shortwave forcing by anthropogenic methane informed by Jovian observations

William D. Collins[1,2]*, Daniel R. Feldman[1], Chaincy Kuo[1], Newton H. Nguyen[3]

Recently, it was recognized that widely used calculations of methane radiative forcing systematically underestimated its global value by 15% by omitting its shortwave effects. We show that shortwave forcing by methane can be accurately calculated despite considerable uncertainty and large gaps in its shortwave spectroscopy. We demonstrate that the forcing is insensitive, even when confronted with much more complete methane absorption spectra extending to violet light wavelengths derived from observations of methane-rich Jovian planets. We undertook the first spatially resolved global calculations of this forcing and find that it is dependent on bright surface features and clouds. Localized annual mean forcing from preindustrial to present-day methane increases approaches +0.25 W/m^2, 10 times the global annualized shortwave forcing and 43% of the total direct CH$_4$ forcing. Shortwave forcing by anthropogenic methane is sufficiently large and accurate to warrant its inclusion in historical analyses, projections, and mitigation strategies for climate change.

INTRODUCTION

Quantification of radiative forcing by anthropogenic well-mixed greenhouse gases (WMGHGs) is required to detect and attribute the historical impacts of these agents on the climate since industrialization and to project their future impacts on Earth's system. The primary role of WMGHGs is to enhance the atmospheric greenhouse effect through absorption and re-emission of terrestrial infrared, or longwave, radiation (1). However, a significant secondary role of the WMGHGs CO$_2$, CH$_4$, and N$_2$O is to absorb incoming solar radiation, thereby heating the atmosphere while simultaneously reducing the surface insolation (2, 3). The shortwave effects of methane have been omitted from the radiative forcing formulae used in past assessments by the Intergovernmental Panel on Climate Change (IPCC) (4, 5). While the forcing formulae have recently been updated to correct this omission (3), those findings raise questions about whether estimates of the forcing by methane will continue to evolve and, if so, by how much. Any overlooked aspects of CH$_4$ absorption could lead to revised radiative forcing estimates with potentially significant ramifications for the relative prioritization both of scientific investigations and of mitigation strategies for anthropogenic WMGHGs.

This paper concerns quantifying two significant uncertainties in the shortwave effects of CH$_4$ and the implications for the estimation of anthropogenic methane radiative forcing. The global uncertainties are associated with the rapidly evolving scientific understanding of CH$_4$ spectroscopy and the regional uncertainties with existing parameterizations of forcing based on limited numbers of radiative transfer calculations. Our incomplete knowledge of methane's absorption features, and hence the uncertainties in our calculations of CH$_4$ shortwave forcing, is due to the remarkable complexity of methane spectroscopic line data (6). Its current derivation from laboratory measurements and theory is known to be seriously incomplete (6–8). Astronomical observations indicate that methane is a broadband solar absorber with absorption bands of widely varying strengths across the visible and near-infrared spectrum, extending to violet light wavelengths at 25,000 cm^{-1} (6–9). However, current spectroscopic

databases informed by laboratory and detailed theoretical calculations, such as the High-Resolution Transmission (HITRAN) (10, 11) and the Gestion et Étude des Informations Spectroscopiques Atmosphériques (GEISA) (12), exhibit shortwave coverage over just the near-infrared absorption features between 3000 and 11,000 cm^{-1}. There are at least three orders of magnitude more absorption lines than are currently tabulated in these databases (6, 10, 12). As these spectroscopic data are the basis for all existing calculations of CH$_4$ shortwave forcing using reference line-by-line (LBL) models (2, 3) and for every shortwave parameterization used in global climate models (13), these calculations and parameterizations all omit the absorption of sunlight by methane at wave numbers greater than 11,000 cm^{-1}.

In principle, this omitted absorption could systematically increase the radiative forcing by CH$_4$. Over 64% (14) of solar insolation occurs at wave numbers $v > 11,000$ cm^{-1}, and hence there is 1.78 times more energy to absorb in this portion of the solar spectrum than at $v \leq 11,000$ cm^{-1}. In addition, several processes including greater Rayleigh scattering (15, 16) and higher cloud and land surface albedos (17, 18) act to increase path lengths traversed by photons with $v > 11,000$ cm^{-1} relative to longer wavelengths. The resulting increase in tropospheric absorption path lengths from increased atmospheric and surface scattering (19, 20) at $v > 11,000$ cm^{-1} reduces the flux of upwelling diffuse solar radiation at the tropopause, thereby potentially increasing the net direct radiative forcing by methane.

RESULTS

We examine the question of whether the shortwave forcing of CH$_4$ is affected by recent and/or future additions to our tabulations of its absorption band structure. First, we examine whether the new CH$_4$ absorption features that have appeared in the HITRAN spectroscopic database (10, 21, 22) since its 2000 edition appreciably alter the direct shortwave forcing at the tropopause. We adopt HITRAN 2000 as the baseline since it was used in the first study to highlight the role of shortwave forcing by methane in climate change simulations (2). HITRAN serves as the source of gaseous absorption spectra for many LBL models (13, 23, 24) and, like GEISA (12), is periodically updated as new measurements and models of these spectra become available. As a result, the maximum wave number at which methane lines have

[1]Lawrence Berkeley National Laboratory, Berkeley, CA 94720, USA. [2]University of California, Berkeley, Berkeley, CA 94720, USA. [3]California Institute of Technology, Pasadena, CA 91125, USA.
*Corresponding author. Email: wdcollins@lbl.gov

Table 1. Direct, instantaneous, unadjusted shortwave radiative forcing by methane (in W/m²) at three atmospheric levels under RTMIP experimental protocol (2). Column-labeled RTMIP shows original RTMIP results (2); columns labeled 2000, 2004, 2008, 2012, and Jovian+2012 show forcings computed using the HITRAN 2000 (21), 2004 (30), 2008 (22), and 2012 (10) databases out to 12,000 cm^{-1} (see Materials and Methods), and the Jovian empirical methane parameterization including parametric uncertainty (2-σ, in parentheses) (9) combined with HITRAN 2012 out to 25,000 cm^{-1} (see Materials and Methods). Rows with units in the Δ column give the differences in forcings relative to the HITRAN 2000 values in absolute and percentage units.

Level	Δ	RTMIP	2000	2004	2008	2012	Jovian+2012
TOA		+0.09	+0.096	+0.098	+0.097	+0.098	+0.099 ± (0.0)
	W/m²			+0.002	+0.002	+0.002	+0.003
	%			+2.064	+1.738	+2.510	+3.349
Tropopause		−0.13	−0.127	−0.132	−0.132	−0.132	−0.132 ± (2.6 × 10^{-8})
	W/m²			−0.005	−0.005	−0.005	−0.005
	%			+4.211	+3.927	+3.978	+3.636
Surface		−0.55	−0.574	−0.589	−0.588	−0.590	−0.594 ± (1.6 × 10^{-8})
	W/m²			−0.015	−0.014	−0.017	−0.020
	%			+2.673	+2.452	+2.889	+3.495

been tabulated has increased almost linearly in time since 1982, while the number of lines has grown exponentially in time (fig. S1). Both HITRAN and GEISA currently include up through the eighth (penta-contakaipentad) polyad between 11,000 and 12,000 cm^{-1}.

Here, we quantify how updates to the HITRAN 2000 edition alter the direct instantaneous shortwave forcing by CH_4. We compute representative forcings by differencing radiative transfer calculations for two numerical experiments conducted under the Radiative Transfer Model Intercomparison Project (RTMIP) (2) protocols for a climatological mid-latitude summer condition (see Materials and Methods). The two experiments are distinguished primarily by differencing well-mixed atmospheric concentrations of CH_4 set to 1760 and 806 parts per billion by volume (ppbv), the conditions for years 2000 and 1860 CE, respectively. As shown in Table 1, recent updates in the spectroscopy perturb the direct instantaneous shortwave forcings from CH_4 in the third decimal place (order 10^{-3} W/m²) at the top of the atmosphere and tropopause and in the second decimal place (order 10^{-2} W/m²) at the surface. These results show that recent spectroscopic updates for CH_4 alter its forcing under the idealized RTMIP protocols by less than approximately 4%.

Second, we investigate whether, in principle, the methane shortwave forcing would change given a comprehensive tabulation of all the major absorption features spanning the Sun's visible and near-infrared spectrum. To accomplish this task, we use an empirical parameterization of methane's absorption optical depth as a function of wave number based on a synthesis of absorption data from observations of Jupiter and Titan (9). The atmospheres of these Jovian planets and moons feature volume mixing ratios of methane that are at least three orders of magnitude greater than those on Earth (25). As a result, absorption features that are too weak to detect in a laboratory can be readily estimated from occultation measurements through Jovian atmospheres. On the basis of these observations, a parameterization of CH_4 absorption has been developed (9) and applied to Earth's atmosphere (see Materials and Methods). The empirical parameterization of this absorption for Earth-like conditions is shown in Fig. 1 and enables us to estimate an upper bound on methane radiative forc-
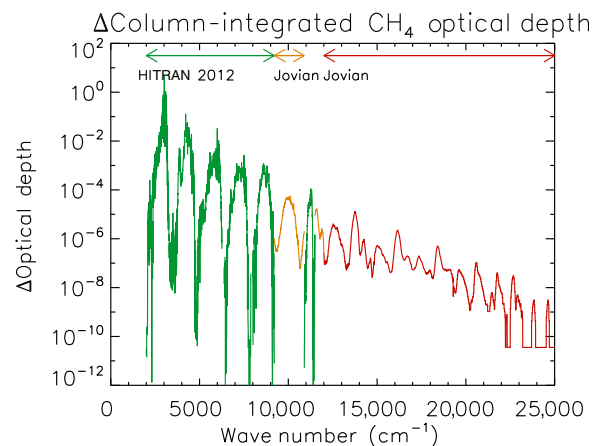

Fig. 1. Difference in CH_4 optical depths between RTMIP experiments 3b and 3d. Green line: Optical depth differences from HITRAN 2012; orange and red lines: optical depth differences computed using the Jovian empirical spectra added to the HITRAN 2012 results for wave numbers below and above 12,000 cm^{-1}, respectively (see Materials and Methods).

ing from possible future additions to laboratory-based tabulations of its absorption lines. Our forcing calculations are summarized in Table 1 and include Jovian absorption spectra for wave numbers between 12,000 and 25,000 cm^{-1}, where laboratory spectroscopic data are not yet available. These results confirm that the idealized RTMIP CH_4 forcings will likely remain stable to two significant figures under future updates to the spectroscopic databases. The addition of the Jovian spectrum does not significantly perturb CH_4 forcings due to the exceptionally low methane absorption optical depths in visible wavelengths (Fig. 1).

On the basis of our observational determination that shortwave CH_4 forcing can be calculated with present spectroscopy, we perform calculations to extend the existing global annual mean estimate (3) so as to include its seasonal cycle, interannual variability, spatial

variability, and sensitivity to surface and atmospheric conditions. We compute the monthly mean, spatially resolved methane forcing from the MODerate resolution atmospheric TRANsmission (MODTRAN) discrete-ordinates radiative transfer code at 15-cm^{-1} resolution using atmospheric state information from climate model simulations for 2006 to 2010 CE that contributed to the Coupled Model Intercomparison Project version 5 (CMIP5) (26) and observational parameterizations of surface radiative boundary conditions (see Materials and Methods). Figure 2 shows the average seasonal cycle, interannual variability, and increase from clear-sky to all-sky conditions in direct shortwave CH_4 forcing at the tropopause. The switch in sign of the clear-sky forcing from negative (Table 1) to positive (Table 2) values is due to the switch from idealized to realistic boundary conditions at the surface and top of the atmosphere, while the switch in sign of the all-sky forcing is also due to the introduction of clouds (3). The increased forcing in the presence of clouds is due to the increased absorption path lengths in methane bands caused by multiple scattering (19, 20). Our global annual mean all-sky forcing of approximately 0.026 W/m^2 agrees with estimates based on weighted averages of

representative atmospheric profiles (3), and our calculations exhibit interannual variability due to variable atmospheric and surface conditions of less than 0.001 W/m^2 (Table 2).

Figure 3A shows that large spatial gradients in shortwave CH_4 forcing are driven by corresponding gradients in low-latitude

A All-sky CH_4 forcing

B Near-IR clear-sky reflected flux

C All-sky forcing cumulative probability

Fig. 3. Annual mean CH_4 shortwave forcings and near-infrared reflected fluxes from the CSIRO Mk3-6-0 (56) ESM. (**A**) CH_4 direct, instantaneous, unadjusted shortwave forcing at the tropopause under all-sky, aerosol-free tropospheric conditions. (**B**) Top-of-atmosphere (TOA) near–infrared (IR) reflected flux under clear-sky, aerosol-free conditions. (**C**) Area-weighted cumulative probability distribution of all-sky CH_4 forcing. Dotted lines denote the point where the forcing exceeds 0, dashed lines denote where the forcing equals the annual mean global all-sky forcing (Table 2), and the circle and cross (plus) symbols and labels denote the mean (maximum) forcing value.
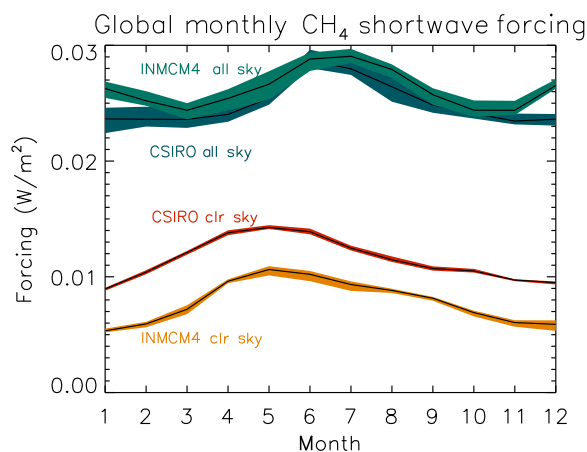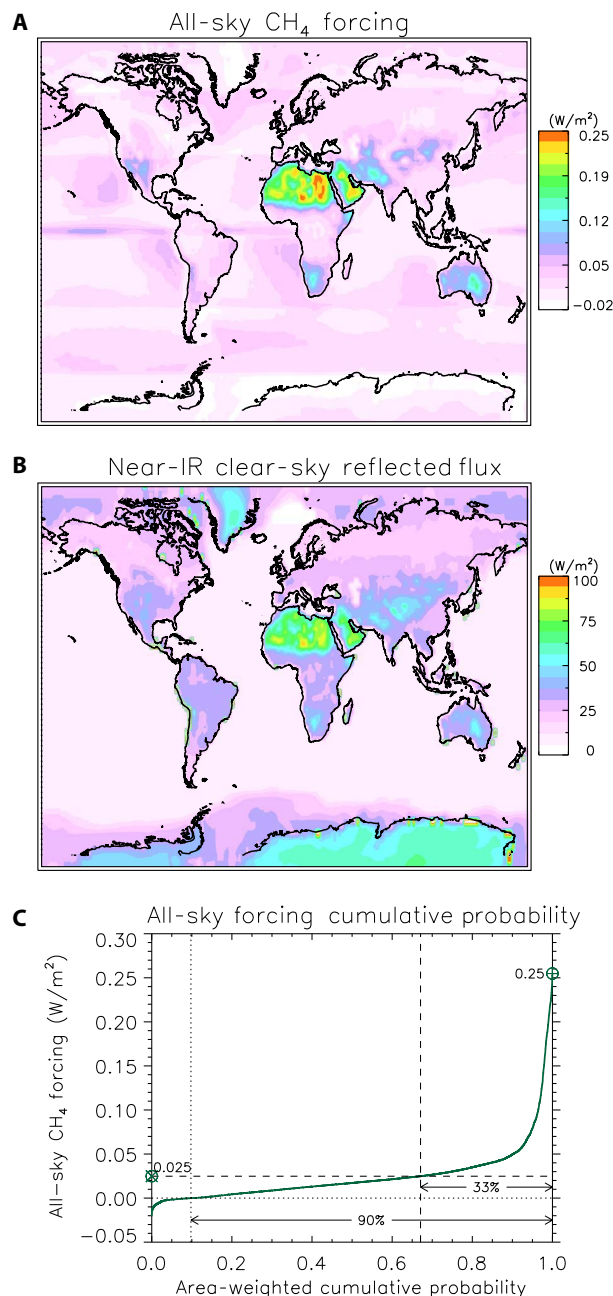
Fig. 2. Monthly mean global direct, instantaneous, unadjusted shortwave radiative forcing at the tropopause from changing tropospheric concentrations of CH_4 from 806 to 1760 ppbv. Solid lines show the mean forcing for each month averaged over 2006 to 2010 CE. Blue and green (red and orange) bands show the range of monthly forcing under all-sky (clear-sky) aerosol-free tropospheric conditions for each individual year using atmospheric state information from the Commonwealth Scientific and Industrial Research Organisation (CSIRO) Mk3-6-0 (56) and INMCM4 (55) Earth System Models (ESMs), respectively (see Materials and Methods).

Table 2. Direct, instantaneous, unadjusted annual mean global shortwave methane radiative forcing at the tropopause under all-sky and clear-sky conditions using atmospheric state information from the CSIRO Mk3-6-0 (56) and INMCM4 (55) ESMs averaged over 2006 to 2010 CE (see Materials and Methods). Uncertainties denote the interannual variability in these forcings.

Condition	Model	Annual mean forcing (W/m²)
All-sky	CSIRO Mk3-6-0	$0.025 \pm (1 \times 10^{-4})$
	INMCM4	$0.026 \pm (4 \times 10^{-4})$
Clear-sky	CSIRO Mk3-6-0	$0.011 \pm (3 \times 10^{-5})$
	INMCM4	$0.008 \pm (2 \times 10^{-4})$

near-infrared surface albedo. Brighter surfaces such as the Sahara Desert and Arabian Peninsula increase photon path lengths in CH_4 absorption bands by reflecting downwelling light upward (Fig. 3B). The maximum localized forcing is +0.25 W/m^2 (Fig. 3C), approximately 10 times the global annualized all-sky shortwave forcing (Table 2).

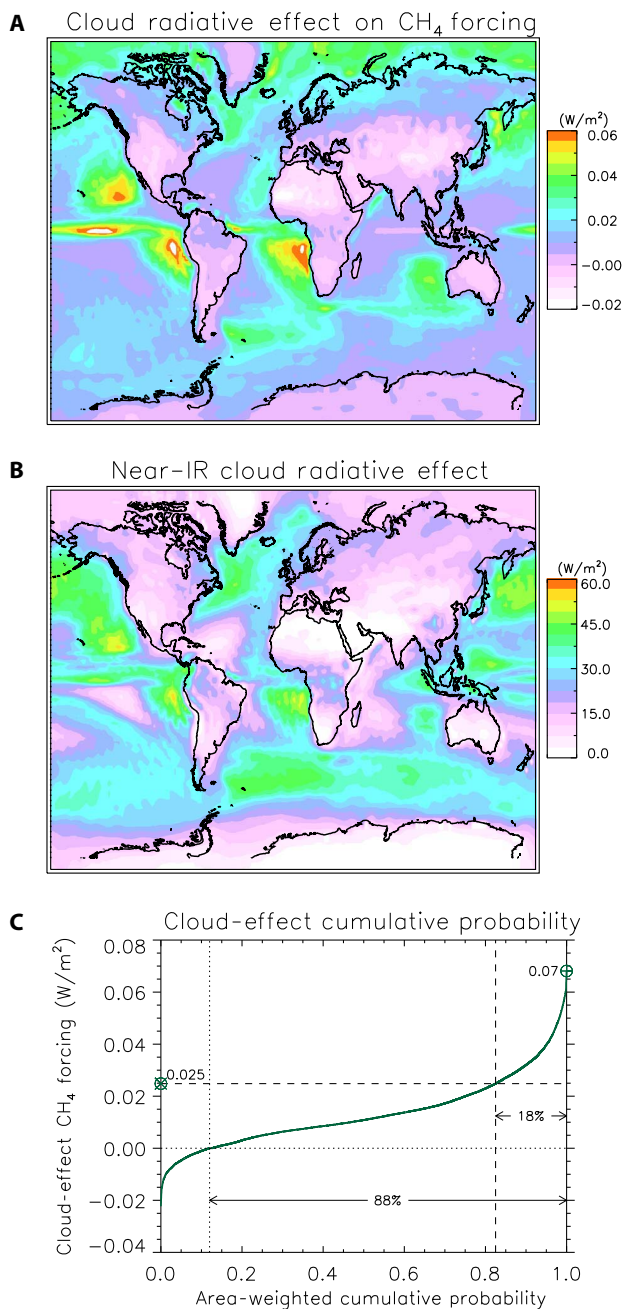**A** Cloud radiative effect on CH$_4$ forcing

(W/m^2)
0.06
0.04
0.02
−0.00
−0.02

B Near−IR cloud radiative effect

(W/m^2)
60.0
45.0
30.0
15.0
0.0

C Cloud-effect cumulative probability

0.07
0.025
18%
88%

Fig. 4. Annual mean enhancements to CH$_4$ shortwave forcings and reflected fluxes by clouds from the CSIRO Mk3-6-0 (56) ESM. (**A**) Difference in CH$_4$ forcing at the tropopause between all-sky and clear-sky aerosol-free tropospheric conditions. (**B**) TOA near-infrared cloud radiative effect. (**C**) Area-weighted cumulative probability distribution of cloud-radiative enhancements. Dotted lines denote the point where the forcing exceeds 0, dashed lines denote where the forcing equals the annual mean global all-sky forcing (Table 2), and the circle and cross (plus) symbols and labels denote the mean (maximum) forcing value.

The local annual mean all-sky forcing is positive over 90% of Earth's surface, and it exceeds the global mean value over 33% of the surface (Fig. 3C). Over the Sahara Desert, where the local maximum in methane forcing occurs, the radiative forcings between 1850 and 2000 CE from ozone, carbonaceous aerosols, and all aerosols are less than or equal to 0.88, 0.88, and 0.12 W/m^2 respectively. In percentage terms, the local methane maximum is approximately 28, 28, and 200% those of ozone, carbonaceous aerosols, and all aerosols, respectively [Fig. 8.23 of (5)].

Figure 4A shows that the local increments in shortwave CH_4 forcing from the presence of clouds are as large as +0.068 W/m^2. The largest increments occur in the same locations as the local maxima in near-infrared cloud radiative effects (Fig. 4B) associated with the oceanic stratus cloud decks west of Southern Africa and North and South America and with the cloud systems in the intertropical convergence zone. High-altitude clouds can reduce the solar flux incident on methane in the lower troposphere and, hence, reduce its forcing relative to clear-sky conditions, but over 88% of Earth's surface, cloud radiative effects act to enhance the methane radiative forcing by up to 2.75 times the global annualized forcing (Fig. 4C).

DISCUSSION

Other sources of error in the calculated direct shortwave CH_4 forcing include uncertain line widths and line strengths for the known lines. These uncertainties perturb the forcing in the third significant figure and, hence, do not appreciably affect our estimates of methane radiative forcing (27). If we combine the sensitivity analyses in this paper with the spectroscopic error analyses (27), then these two studies demonstrate that calculations of shortwave CH_4 forcing based on current tabulations of methane absorption lines are certain to two significant figures. Therefore, shortwave terms recently added to the IPCC forcing formulae (3), and the associated upward revision of methane's global warming potential and global temperature potential should be regarded as sufficiently accurate for applications to the climate system into the foreseeable future, starting with, but not limited to, the upcoming IPCC Sixth Assessment Report.

MATERIALS AND METHODS
Quantification of spectroscopic uncertainty in direct CH$_4$ forcing

The methods used in this study are based on three components: experimental protocols, tabulation of methane absorption spectra, and models that are all used in combination to calculate the shortwave direct radiative forcing by CH_4. The calculations were designed to compute the direct and unadjusted shortwave forcing due to an increase in CH_4 concentrations from 806 to 1760 ppbv under idealized cloud- and aerosol-free clear-sky conditions.

The protocols we adopted are identical to those for experiments 3b and 3d from the RTMIP (2). Experiment 3b corresponds to present-day greenhouse gas (GHG) concentrations in 2000 CE, while experiment 3d corresponds to a counterfactual atmosphere with CH_4, CFC-11, and CFC-12 set to their concentrations in 1860 CE while other atmospheric properties are held at present-day climatological values. Since the methane concentrations in these two experiments are 1760 and 806 ppbv, respectively, differencing the radiative fluxes calculated for these experiments provides an estimate of the direct shortwave forcing by CH_4 between 2000 and 1860 CE. Following RTMIP,

the upper boundary conditions are a TOA solar insolation (28) of 1360 W/m^2 and a solar zenith angle of 53°. The lower boundary condition is a Lambertian surface with a spectrally flat albedo of 0.1. The atmospheric thermodynamic conditions and water vapor and ozone mixing ratios correspond to the Air Force Geophysics Laboratory (AFGL) mid-latitude summer atmospheric profile (29) interpolated onto 458 vertical levels extending from the surface at 1011.4 hPa to the effective top of the atmosphere at 0.0 hPa. This is the same atmospheric profile used for the LBL calculations in RTMIP.

The first set of LBL calculations is based on HITRAN editions 2000 (21), 2004 (30), 2008 (22), and 2012 (10). The HITRAN 2000 data set included methane lines up through the fourth polyad, or tetradecad (6), at approximately 6000 cm^{-1}; HITRAN 2004 included new lines between 6180 and 9200 cm^{-1}; whereas HITRAN 2008 added the fifth (icosad) and sixth (triacontad) polyads at ~7500 and 9000 cm^{-1}. The HITRAN 2012 data set added the eighth (pentacontakaipentad) polyad between 11,000 and 12,000 cm^{-1} while skipping the seventh (tetracontad) polyad spanning 10,000 cm^{-1}, although this missing polyad has subsequently been measured in the laboratory (31) and has been included in the 2016 HITRAN edition. As of this writing, the most recent HITRAN 2016 update (11) to CH$_4$ spectroscopy is still not fully implemented in the LBL code described below, and therefore, we have not included it in our calculations.

The second set of LBL calculations is based on CH$_4$ spectral optical properties from compilations of measurements of the Jovian planetary atmospheres (9). The optical depths $\tau(v)$ as functions of wave number v were computed using the Voigt-Goody model following

$$\tau(v) = 2\kappa(v, T)w \int_0^\infty V(x, y) \bigg/ \left[1 + \kappa(v, T)w(\delta/\alpha_D^0)_v V(x, y)/\sqrt{T}\right] dx \quad (1)$$

$$V(x, y) = y\pi^{-3/2} \int_{-\infty}^\infty \exp(-t^2) \bigg/ \left[y^2 + (x - t)^2\right] dt \quad (2)$$

$$y = (\alpha_L^0/\alpha_D^0)(P/P_0)\left(\sqrt{T_0}/T\right)[q + (1 - q)/\text{SFB}] \quad (3)$$

where $\kappa(v, T)$ is the spectrally varying absorption coefficient at temperature T, w is the integrated methane amount per unit area (in kilometer-amagats equal to 4.4615 mol/cm^2), $(\delta/\alpha_D^0)_v$ is the wave number–dependent ratio of the mean line spacing to Doppler line width, $V(x, y)$ is the Voigt function, (α_L^0/α_D^0) is the ratio of Lorentz and Doppler line widths, P is the pressure, q is the methane mole fraction, SFB is the dimensionless self-to-foreign broadening coefficient, and reference conditions are T_0 = 296 K and P_0 = 1.01325 bars. The temperature dependence of $\kappa(v, T)$ is parameterized using (9)

$$\log_e[\kappa(v, T)] = 0.5z(z - 1)\log_e[\kappa(v, 100)] +$$
$$(1 - z^2)\log_e[\kappa(v, 198)] + 0.5z(z + 1)\log_e[\kappa(v, 296)] \quad (4)$$

$$z = (T - 198)/98 \quad (5)$$

Computing $\tau(v)$ requires (i) vertical profiles of P, T, q, and w; (ii) tables of $\kappa(v, 100)$, $\kappa(v, 198)$, and $\kappa(v, 296)$ as functions of v to compute $\kappa(v, T)$ from Eq. 4; (iii) a tabulation of $(\delta/\alpha_D^0)_v$ versus v; and (iv) values for the free parameters (α_L^0/α_D^0) and SFB. Inputs (ii) and

(iii) are available from optical measurements of Jovian planetary atmospheres (9). The line width ratio (32) (α_L^0/α_D^0) varies between 120 and 200 K$^{1/2}$, and we performed the calculations at these bounding values and the best fit value (9) of 150 K$^{1/2}$. The self-broadening parameter SFB varies (33) between 1.2 and 1.5, and we again performed the calculations at these bounding values and the best fit value (9) of 1.4. We integrated these equations using the DQAGI numerical quadrature routines from the SLATEC (Sandia, Los Alamos, Air Force Weapons Laboratory Technical Exchange Committee) Fortran library (34).

We input the atmospheric profiles and HITRAN line databases into an LBL radiative transfer code to calculate the vertically and spectrally resolved profiles of absorption optical depths summed over H$_2$O, CO$_2$, CH$_4$, and O$_3$. We used the Line-By-Line Radiative Transfer Model (LBLRTM) (13) version 12.2 to perform these calculations for HITRAN 2000, 2004, and 2008 and version 12.4 for HITRAN 2012. The switch to the newer version was necessitated by the new line mixing specification parameters starting in HITRAN 2012 (35). The treatments of the water vapor continuum in LBLRTM versions 12.2 and 12.4 are the Mlawer-Tobin-Clough-Kneizys-Davies (MT_CKD) parameterizations (36) versions 2.5.2 and 2.7, respectively.

We used a spectral resolution of δv = 0.0001 cm^{-1}, sufficient to resolve 99% of the very narrow H$_2$O absorption lines in the stratosphere at pressures above 0.01 atmosphere (37), and a spectral range of 2000 to 34,000 cm^{-1} covering 98.6% of TOA insolation. The resulting tables of absorption optical depth contain 3.2×10^8 spectral intervals times 458 vertical levels and are therefore much too large for practical calculations of radiative flux profiles. For this reason, we constructed transmission weighted average optical depths for subsequent radiative calculations at a much lower spectral resolution of $\delta\bar{v}$ = 5 cm^{-1}. Let i denote the ith averaged and j denote the jth original high-resolution optical depth summed over H$_2$O, CO$_2$, CH$_4$, and O$_3$, respectively. Then, the averaged optical depth was computed by

$$\bar{\tau}(\bar{v}_i) = -\ln\left\{\frac{1}{N} \sum_{j=iN}^{(i+1)N-1} \exp[-\tau(v_j)]\right\} \quad (6)$$

$$N = \frac{\delta\bar{v}}{\delta\bar{v}} \quad (7)$$

$$\bar{v}_i = v_{iN} + \frac{N}{2}\delta v \quad (8)$$

By construction, each averaged optical depth yields the same transmission through a given layer as the mean of the transmissions for the N high-resolution spectral intervals used in its calculation. Because of the very large optical depths that can exceed 10^4 in the primary absorption band of H$_2$O at v = 3730 cm^{-1} and its overtone bands in the near-infrared (37), the calculations in Eq. 6 require nonstandard numerical precision. In standard single or double precision computer arithmetic, the transmissions corresponding to these very large optical depths will underflow and be set to zero. However, in quadruple precision computer arithmetic, the smallest number that can be represented is roughly

$$2^{-2^{14}} = 2^{-16384} = e^{-16384*\ln(2)} \simeq e^{-11356} \quad (9)$$

so optical depths up to $\tau(v_j) \lesssim 11356$ can be accommodated. Therefore, we adopted quadruple (or "quad") precision arithmetic to

compute averaged optical depths from the high-spectral-resolution optical depths without underflowing.

We used the Discrete Ordinates Radiative Transfer (DISORT) code (38) version 2 in a massively parallel implementation (37) to compute the fluxes corresponding to RTMIP experiments 3b and 3d. Our algorithm combines the average optical depths from Eq. 6 with scattering optical depths for Rayleigh scattering (15) and inputs the resulting extinction optical depths into a reentrant, thread-safe implementation of DISORT2. For these calculations, we used eight streams and set the TOA solar flux to standard spectra (14).

Results for sensitivity of CH₄ forcing to recent spectroscopic database updates

The impacts of recent updates to methane spectral data are evident in both the methane absorption optical depths and in the methane direct radiative forcing. The increase in the column-integrated $\delta\bar{\tau}(v)$ when CH_4 concentrations increase from 806 to 1760 ppbv is shown in fig. S2, as calculated using HITRAN 2000 applied to RTMIP experiments 3b and 3d. The increments to this calculation using subsequent HITRAN editions are shown in fig. S3. These increments are one to two orders of magnitude smaller than the $\delta\bar{\tau}(v)$, and we would therefore anticipate that the increments to the resulting forcings would also be one to two orders of magnitude smaller based on the single-scattering linear limit of the solution to the radiative transfer equations. This expectation is borne out by the full forcing calculations shown in fig. S4, which show perturbations at TOA and the tropopause of $O(10^{-3})$ W/m² and at the surface of $O(10^{-2})$ W/m². The results for the direct shortwave methane forcing computed by differencing RTMIP experiments 3b and 3d are shown in Table 1 for the three versions of HITRAN. The additional polyads and changes in previously characterized polyads change the TOA, tropopause, and surface forcings all by less than 4%.

Results for sensitivity of CH₄ forcing to inclusion of Jovian spectral parameters

We used the parameterization of Jovian absorption spectra to extend $\delta\bar{\tau}(v)$ from the laboratory upper wave number bound $v \le 12{,}000$ cm⁻¹ to the Jovian bound $v \le 25{,}000$ cm⁻¹, that is, the color violet at a wavelength of 400 nm. The orange and red lines in Fig. 1 show the column-integrated change in optical depth computed using the Jovian parameterization for an increase in CH_4 concentrations from 806 to 1760 ppbv under the RTMIP protocol. To ensure that the results are robust to the uncertainties in the disposable parameters (α_L^0/α_D^0) and SFB, we sequentially assigned trios of low, central, and high values to both parameters and computed $\delta\bar{\tau}(v)$ and the forcings for all nine possible pairs of values from the two trios. For (α_L^0/α_D^0), we used 120, 150, and 200 K^{1/2} for the value trio (9), and for SFB, we adopted 1, 2, 1.4, and 1.5 for the value trio (33). The forcings for the nine parameter combinations given in Table 1 show that the additional absorption by the CH_4 polyads at wave numbers above 12,000 cm⁻¹ only perturbs the forcings at the third or fourth significant figure at TOA and the tropopause, respectively. These findings do not change when the calculation is repeated using a Lambertian surface albedo of 0.3, close to the global annual mean albedo of Earth (39).

Calculation of spatially resolved CH₄ forcing

The spatial maps of CH_4 forcing in Figs. 3 and 4 were computed from climate model output from the CMIP5 (26) using the Observing System Simulation Experiment (OSSE) framework developed by the

authors (40–42) for NASA's CLimate Absolute Radiance and Refractivity Observatory (CLARREO) (43) and validated against SCanning Imaging Absorption SpectroMeter for Atmospheric CHartographY (SCIAMACHY) satellite observations (44, 45).

The OSSE framework ingests time-dependent two- and three-dimensional climate model outputs that, when combined with auxiliary initial and boundary conditions and other data sets, provide a complete prescription of the climate system state required to compute the vertically resolved radiation fields throughout the atmosphere at each model grid point and time interval. The computations were performed using the MODTRAN code version 5.3.0.0. The MODTRAN calculations were performed using the DISORT code (38) with eight streams at 15-cm⁻¹ resolution over a spectral range of 2000 to 11,900 cm⁻¹. The spectral properties of radiative active gases in MODTRAN version 5.3.0.0 were obtained from HITRAN 2008 (22). HITRAN's description of CH_4 line absorption parameters has been updated substantially in recent versions (6) (46). Recent laboratory and theoretical work led to updates to over 70% of the lines in the HITRAN 2012 database. However, calculations based on the HITRAN 2012 database exhibited larger discrepancies with respect to high-altitude balloon (47) and satellite validation measurements (48). We therefore chose to use the HITRAN 2008 spectroscopy because the 2012 update agrees less favorably with observations and because the 2016 update has yet to be implemented fully into the OSSE framework at the time of this writing.

The radiative quantities computed by MODTRAN include the spectral and spectrally integrated fluxes under clear-sky and all-sky conditions at all levels in the input model fields. The fluxes are further separated into the downwelling direct, downward diffuse, and upwelling diffuse terms. The MODTRAN calculations for RTMIP differ with the LBL calculations using the HITRAN 2012 line database by −0.016 W/m² at the surface, +0.017 W/m² at the tropopause, and +0.003 W/m² at the top of model (TOM). For comparison, the SDs of the forcing among the LBL codes that participated in RTMIP are, to two decimal places, 0.02 W/m² at the surface, 0.00 W/m² at the tropopause, and 0.00 W/m² at the TOM. This demonstrated that the MODTRAN code is performing comparably to the much more computationally expensive LBL codes.

When clouds are present in a model column, grid-point-mean fluxes are computed assuming maximum-random cloud overlap in the vertical direction by adopting the independent column approximation and generating a set of binary cloud configurations that aggregate to the original model profile of cloud amount (49). Radiative transfer calculations were performed for each binary cloud configuration and combined in a sum weighted by the fractional areas occupied by each configuration within the grid cell (49). When sea ice was present, the full set of clear-sky and all-sky calculations was repeated for 100% open-ocean and 100% sea ice–covered conditions and then combined in a sum weighted by the fractional sea ice coverage. This approach accurately accounts for nonlinear effects of multiple scattering of sunlight between ice and overlying clouds.

The upper boundary condition on the calculations was the incident solar insolation on the TOA and was obtained from the Kurucz solar spectrum (14) where all values were uniformly scaled such that the TOA irradiance (28) is 1360 W/m². The lower boundary conditions were surface albedos derived from observations rather than obtained from the climate models to maximize the physical fidelity of the surface spectral properties (fig. S5A) (40, 41). The land surface and snow albedos were obtained from climate model grid spectral seven-band

Moderate Resolution Imaging Spectroradiometer (MODIS) bi-directional reflectance distribution functions (BRDFs) (50), ocean albedos were derived from the Cox-Munk ocean BRDF (51), and sea ice albedos were obtained from the Ross-Li BRDF model (52) calibrated against bare sea ice optical data (53). Separate snow-free and completely snow-covered BRDFs were constructed at each grid point, were combined to account for time-varying snow coverage, and were the source of most of the interannual variability in the near-infrared surface albedo (fig. S5B).

The climate model simulations used were for present-day segments of the Representative Concentration Pathway 8.5 CMIP5 scenario (54) runs from the CMIP5 (26) produced by the INMCM4 (55) and CSIRO Mk3-6-0 (56) ESMs for the r1i1p1 (57) and r4i1p1 (57) ensemble members, respectively. These models were chosen because their climate sensitivities roughly span the range diagnosed across the CMIP5 ensemble and also have highly contrasting shortwave cloud radiative effects (58). The time resolution of the climate model output is monthly, and the time period selected for analysis here spans five full years from January 2006 through December 2010. The input fields are detailed in table S1. The calculations were performed at two globally uniform tropospheric CH_4 concentrations of 806 and 1760 ppbv with vertical meridionally dependent gradients in the stratosphere (59). For each of these concentrations, for each month, the fluxes were computed for globally uniform solar zenith angles specified by a standard seven-point Gauss-Legendre quadrature over 0° to 90° zenith angle. The weights in the quadrature formulae required to compute diurnally averaged fluxes at each model grid point are functions of month and latitude. These weights were computed from cumulative probability distributions of solar zenith angles constructed using calculations of the Sun-Earth viewing geometry at a 1-min frequency using the same solar ephemeris used in the Community Atmospheric Model version 3 (60).

SUPPLEMENTARY MATERIALS

Supplementary material for this article is available at http://advances.sciencemag.org/cgi/content/full/4/9/eaas9593/DC1

Fig. S1. Time evolution of CH_4 spectroscopic properties catalogued in the HITRAN databases.
Fig. S2. Change in column-integrated CH_4 optical depth between RTMIP experiments 3b (2000 CE conditions) and 3d (1860 CE conditions) using the HITRAN 2000 line database.
Fig. S3. Perturbations to changes in column-integrated CH_4 optical depth between RTMIP experiments 3b and 3d.
Fig. S4. Cumulative perturbations to changes in CH_4 direct, instantaneous, unadjusted spectral forcing between RTMIP experiments 3b and 3d due to substituting the HITRAN 2004, 2008, and 2012 line databases for the HITRAN 2000 line database.
Fig. S5. Near-infrared black-sky surface albedo retrieved from MODIS for 2003 to 2014 CE.
Table S1. The variable names, source model components, and descriptive names of the monthly mean fields used as input to the OSSE from the CMIP.

REFERENCES AND NOTES

1. R. Pierrehumbert,Infrared radiation and planetary temperature. *Phys. Today* **64**, 33–38 (2011).
2. W. D. Collins, V. Ramaswamy, M. D. Schwarzkopf, Y. Sun, R. W. Portmann, Q. Fu, S. E. B. Casanova, J.-L. Dufresne, D. W. Fillmore, P. M. D. Forster, V. Y. Galin, L. K. Gohar, W. J. Ingram, D. P. Kratz, M.-P. Lefebvre, J. Li, P. Marquet, V. Oinas, Y. Tsushima, T. Uchiyama, W. Y. Zhong, Radiative forcing by well-mixed greenhouse gases: Estimates from climate models in the Intergovernmental Panel on Climate Change (IPCC) Fourth Assessment Report (AR4). *J. Geophys. Res.* **111**, D14317 (2006).
3. M. Etminan, G. Myhre, E. J. Highwood, K. P. Shine, Radiative forcing of carbon dioxide, methane, and nitrous oxide: a significant revision of the methane radiative forcing. *Geophys. Res. Lett.* 43, 12614–12623 (2016).
4. P. Forster,V. Ramaswamy, P. Artaxo, T. Berntsen, R. Betts, D. W. Fahey, J. Haywood, J. Lean, D. C. Lowe, G. Myhre, J. Nganga, R. Prinn, G. Raga, M. Schulz, R. Van Dorland, Changes in

atmospheric constituents and in radiative forcing, in *Climate Change 2007: The Physical Science Basis. Contribution of Working Group I to the Fourth Assessment Report of the Intergovernmental Panel on Climate Change*, S. Solomon, D. Qin, M. Manning, Z. Chen, M. Marquis, K. B. Averyt, M. Tignor, H. L. Miller, Eds. (Cambridge Univ. Press, 2007), chap. 2, pp. 129–234.
5. G. Myhre, D. Shindell, F.-M. Bréon, W. Collins, J. Fuglestvedt, J. Huang, D. Koch, J.-F. Lamarque, D. Lee, B. Mendoza, T. Nakajima, A. Robock, G. Stephens, T. Takemura, H. Zhang, Anthropogenic and natural radiative forcing, in *Climate Change 2013: The Physical Science Basis. Contribution of Working Group I to the Fifth Assessment Report of the Intergovernmental Panel on Climate Change*, T. F. Stocker, D. Qin, G.-K. Plattner, M. Tignor, S.K. Allen, J. Doschung, A. Nauels, Y. Xia, V. Bex, P. M. Midgley, Eds. (Cambridge Univ. Press, 2013), chap. 8, pp. 659–740.
6. L. R. Brown, K. Sung, D. C. Benner, V. M. Devi, V. Boudon, T. Gabard, C. Wenger, A. Campargue, O. Leshchishina, S. Kassi, D. Mondelain, L. Wang, L. Daumont, L. Régalia, M. Rey, X. Thomas, V. G. Tyuterev, O. M. Lyulin, A. V. Nikitin, H. M. Niederer, S. Albert, S. Bauerecker, M. Quack, J. J. O'Brien, I. E. Gordon, L. S. Rothman, H. Sasada, A. Coustenis, M. A. H. Smith, T. Carrington, X. G. Wang, A. W. Mantz, P. T. Spickler, Methane line parameters in the HITRAN2012 database. *J. Quant. Spectrosc. Radiat. Transf.* **130**, 201–219 (2013).
7. R. Checa-Garcia, J. Landgraf, A. Galli, F. Hase, V. A. Velazco, H. Tran, V. Boudon, F. Alkemade, A. Butz, Mapping spectroscopic uncertainties into prospective methane retrieval errors from Sentinel-5 and its precursor. *Atmos. Meas. Tech.* **8**, 3617–3629 (2015).
8. T. Delahaye, S. E. Maxwell, Z. D. Reed, H. Lin, J. T. Hodges, K. Sung, V. M. Devi, T. Warneke, P. Spietz, H. Tran, Precise methane absorption measurements in the 1.64 µm spectral region for the MERLIN mission. *J. Geophys. Res.* **121**, 7360–7370 (2016).
9. E. Karkoschka, M. G. Tomasko, Methane absorption coefficients for the jovian planets from laboratory, Huygens, and HST data. *Icarus* **205**, 674–694 (2010).
10. L. S. Rothman, I. E. Gordon, Y. Babikov, A. Barbe, D. Chris Benner, P. F. Bernath, M. Birk, L. Bizzocchi, V. Boudon, L. R. Brown, A. Campargue, K. Chance, E. A. Cohen, L. H. Coudert, V. M. Devi, B. J. Drouin, A. Fayt, J.-M. Flaud, R. R. Gamache, J. J. Harrison, J.-M. Hartmann, C. Hill, J. T. Hodges, D. Jacquemart, A. Jolly, J. Lamouroux, R. J. Le Roy, G. Li, D. A. Long, O. M. Lyulin, C. J. Mackie, S. T. Massie, S. Mikhailenko, H. S. P. Müller, O. V. Naumenko, A. V. Nikitin, J. Orphal, V. Perevalov, A. Perrin, E. R. Polovtseva, C. Richard, M. A. H. Smith, E. Starikova, K. Sung, S. Tashkun, J. Tennyson, G. C. Toon, V. G. Tyuterev, G. Wagner, The HITRAN2012 molecular spectroscopic database. *J. Quant. Spectrosc. Radiat. Transf.* **130**, 4–50 (2013).
11. I. E. Gordon, I. E. Gordon, L. S. Rothman, C. Hill, R. V. Kochanov, Y. Tan, P. F. Bernath, M. Birk, V. Boudon, A. Campargue, K. V. Chance, B. J. Drouin, J.-M. Flaud, R. R. Gamache, J. T. Hodges, D. Jacquemart, V. I. Perevalov, A. Perrin, K. P. Shine, M.-A. H. Smith, J. Tennyson, G. C. Toon, H. Tran, V. G. Tyuterev, A. Barbe, A. G. Császár, V. M. Devi, T. Furtenbacher, J. J. Harrison, J.-M. Hartmann, A. Jolly, T. J. Johnson, T. Karman, I. Kleiner, A. A. Kyuberis, J. Loos, O. M. Lyulin, S. T. Massie, S. N. Mikhailenko, N. Moazzen-Ahmadi, H. S. P. Müller, O. V. Naumenko, A. V. Nikitin, O. L. Polyansky, M. Rey, M. Rotger, S. W. Sharpe, K. Sung, E. Starikova, S. A. Tashkun, J. Vander Auwera, G. Wagner, J. Wilzewski, P. Wcisło, S. Yu, E. J. Zak, The HITRAN2016 molecular spectroscopic database. *J. Quant. Spectrosc. Radiat. Transf.* **203**, 3–69 (2017).
12. N. Jacquinet-Husson, R. Armante, N. A. Scott, A. Chédin, L. Crépeau, C. Boutammine, A. Bouhdaoui, C. Crevoisier, V. Capelle, C. Boonne, N. Poulet-Crovisier, A. Barbe, D. Chris Benner, V. Boudon, L. R. Brown, J. Buldyreva, A. Campargue, L. H. Coudert, V. M. Devi, M. J. Down, B. J. Drouin, A. Fayt, C. Fittschen, J.-M. Flaud, R. R. Gamache, J. J. Harrison, C. Hill, Ø. Hodnebrog, S.-M. Hu, D. Jacquemart, A. Jolly, E. Jiménez, N. N. Lavrentieva, A.-W. Liu, L. Lodi, O. M. Lyulin, S. T. Massie, S. Mikhailenko, H. S. P. Müller, O. V. Naumenko, A. Nikitin, C. J. Nielsen, J. Orphal, V. I. Perevalov, A. Perrin, E. Polovtseva, A. Predoi-Cross, M. Rotger, A. A. Ruth, S. S. Yu, K. Sung, S. A. Tashkun, J. Tennyson, V. G. Tyuterev, J. Vander Auwera, B. A. Voronin, A. Makie, The 2015 edition of the GEISA spectroscopic database. *J. Mol. Spectrosc.* **327**, 31–72 (2016).
13. S. A. Clough, M. W. Shephard, E. J. Mlawer, J. S. Delamere, M. J. Iacono, K. Cady-Pereira, S. Boukabara, P. D. Brown, Atmospheric radiative transfer modeling: A summary of the AER codes. *J. Quant. Spectrosc. Radiat. Transf.* **91**, 233–244 (2005).
14. R. L. Kurucz, The solar irradiance by computation, in *Proceedings of the 17th Annual Review Conference on Atmospheric Transmission Models, Special Reports, No. 274*, G. P. Anderson, R. H. Picard, J. H. Chetwynd, Eds. (Phillips Laboratory, Hanscomb AFB, Mass., 1995).
15. J. Lenoble, *Atmospheric Radiative Transfer (Studies in Geophysical Optics and Remote Sensing)* (A. Deepak Pub., 1993).
16. K. Pfeilsticker, F. Erie, O. Funk, H. Veitel, U. Platt, First geometrical pathlengths probability density function derivation of the skylight from spectroscopically highly resolving oxygen A-band observations: 1. Measurement technique, atmospheric observations and model calculations. *J. Geophys. Res.* **103**, 11483–11504 (1998).
17. F.-L. Chang, Z. Li, A near-global climatology of single-layer and overlapped clouds and their optical properties retrieved from Terra/MODIS data using a new algorithm. *J. Climate* **18**, 4752–4771 (2005).

18. K. W. Oleson, G. B. Bonan, C. Schaaf, F. Gao, Y. Jin, A. Strahler, Assessment of global climate model land surface albedo using MODIS data. *Geophys. Res. Lett.* **30**, 1443 (2003).

19. H. Veitel, O. Funk, C. Kurz, U. Platt, K. Pfeilsticker, Geometrical path length probability density function of the skylight transmitted by midlatitude cloudy skies: Some case studies. *Geophys. Res. Lett.* **25**, 3355–3358 (1998).

20. O. Funk, K. Pfeilsticker, Photon path length distributions for cloudy skies—Oxygen A-Band measurements and model calculations. *Ann. Geophys.* **21**, 615–626 (2003).

21. L. S. Rothman, A. Barbe, D. Chris Benner, L. R. Brown, C. Camy-Peyret, M. R. Carleer, K. Chance, C. Clerbaux, V. Dana, V. M. Devi, A. Fayt, J.-M. Flaud, R. R. Gamache, A. Goldman, D. Jacquemart, K. W. Jucks, W. J. Lafferty, J.-Y. Mandin, S. T. Massie, V. Nemtchinov, D. A. Newnham, A. Perrin, C. P. Rinsland, J. Schroeder, K. M. Smith, M. A. H. Smith, K. Tang, R. A. Toth, J. Vander Auwera, P. Varanasi, K. Yoshino, The HITRAN molecular spectroscopic database: Edition of 2000 including updates through 2001. *J. Quant. Spectrosc. Radiat. Transf.* **82**, 5–44 (2003).

22. L. S. Rothman, I. E. Gordon, A. Barbe, D. Chris Benner, P. F. Bernath, M. Birk, V. Boudon, L. R. Brown, A. Campargue, J.-P. Champion, K. Chance, L. H. Coudert, V. Dana, V. M. Devi, S. Fally, J.-M. Flaud, R. R. Gamache, A. Goldman, D. Jacquemart, I. Kleiner, N. Lacome, W. J. Lafferty, J.-Y. Mandin, S. T. Massie, S. N. Mikhailenko, C. E. Miller, N. Moazzen-Ahmadi, O. V. Naumenko, A. V. Nikitin, J. Orphal, V. I. Perevalov, A. Perrin, A. Predoi-Cross, C. P. Rinsland, M. Rotger, M. Šimečková, M. A. H. Smith, K. Sung, S. A. Tashkun, J. Tennyson, R. A. Toth, A. C. Vandaele, J. Vander Auwera, The HITRAN 2008 molecular spectroscopic database. *J. Quant. Spectrosc. Radiat. Transf.* **110**, 533–572 (2009).

23. A. Berk, G. P. Anderson, P. K. Acharya, L. S. Bernstein, L. Muratov, J. Lee, M. J. Fox, S. M. Adler-Golden, J. H. Chetwynd, M. L. Hoke, R. B. Lockwood, T. W. Cooley, J. A. Gardner, MODTRAN5: A reformulated atmospheric band model with auxiliary species and practical multiple scattering options. *Proc. SPIE* **5655**, 88–95 (2005).

24. A. Dudhia, The Reference Forward Model (RFM). *J. Quant. Spectrosc. Radiat. Transf.* **186**, 243–253 (2017).

25. I. de Pater, J. Lissauer, *Planetary Sciences* (Cambridge Univ. Press, ed. 2, 2015).

26. K. E. Taylor, R. J. Stouffer, G. A. Meehl, An overview of CMIP5 and the experiment design. *Bull. Am. Meteorol. Soc.* **93**, 485–498 (2012).

27. D. Feldman, et al., *Journal of Quantitative Spectroscopy and Radiative Transfer TBD*, (TBD, 2017).

28. G. Kopp, J. L. Lean, A new, lower value of total solar irradiance: Evidence and climate significance. *Geophys. Res. Lett.* **38**, L01706 (2011).

29. G. P. Anderson, S. A. Clough, F. Kneizys, J. Chetwynd, E. P. Shettle, "AFGL atmospheric constituent profiles (0-120km)" (Technical Report AFGL-TR 86-0110, Optical Physics Division, Air Force Geophysics Laboratory, Hanscom AFB, MA, 1986).

30. L. S. Rothman, D. Jacquemart, A. Barbe, D. Chris Benner, M. Birk, L. R. Brown, M. R. Carleer, C. Chackerian Jr., K. Chance, L. H. Coudert, V. Dana, V. M. Devi, J.-M. Flaud, R. R. Gamache, A. Goldman, J.-M. Hartmann, K. W. Jucks, A. G. Maki, J.-Y. Mandin, S. T. Massie, J. Orphal, A. Perrin, C. P. Rinsland, M. A. H. Smith, J. Tennyson, R. N. Tolchenov, R. A. Toth, J. Vander Auwera, P. Varanasi, G. Wagner, The HITRAN 2004 molecular spectroscopic database. *J. Quant. Spectrosc. Radiat. Transf.* **96**, 139–204 (2005).

31. S. Béguier, A. W. Liu, A. Campargue, An empirical line list for methane near 1 μm (9028–10,435 cm^{-1}). *J. Quant. Spectrosc. Radiat. Transf.* **166**, 6–12 (2015).

32. K. Strong, F. W. Taylor, S. B. Calcutt, J. J. Remedios, J. Ballard, Spectral parameters of self- and hydrogen-broadened methane from 2000 to 9500 cm^{-1} for remote sounding of the atmosphere of Jupiter. *J. Quant. Spectrosc. Radiat. Transf.* **50**, 363–429 (1993).

33. P. G. J. Irwin, L. A. Sromovsky, E. K. Strong, K. Sihra, N. A. Teanby, N. Bowles, S. B. Calcutt, J. J. Remedios, Improved near-infrared methane band models and k-distribution parameters from 2000 to 9500 cm^{-1} and implications for interpretation of outer planet spectra. *Icarus* **181**, 309–319 (2006).

34. W. H. Vandevender, K. H. Haskell, The SLATEC mathematical subroutine library. *ACM SIGNUM Newslett.* **17**, 16–21 (1982).

35. F. Niro, K. Jucks, J.-M. Hartmann, Spectra calculations in central and wing regions of CO_2 IR bands. IV: Software and database for the computation of atmospheric spectra. *J. Quant. Spectrosc. Radiat. Transf.* **95**, 469–481 (2005).

36. E. J. Mlawer, V. H. Payne, J.-L. Moncet, J. S. Delamere, M. J. Alvarado, D. C. Tobin, Development and recent evaluation of the MT_CKD model of continuum absorption. *Philos. Trans. R. Soc. A Math. Phys. Eng. Sci.* **370**, 2520–2556 (2012).

37. W. D. Collins, J. M. Lee-Taylor, D. P. Edwards, G. L. Francis, Effects of increased near-infrared absorption by water vapor on the climate system. *J. Geophys. Res.* **111**, D18109 (2006).

38. K. Stamnes, S.-C. Tsay, W. Wiscombe, K. Jayaweera, Numerically stable algorithm for discrete-ordinate-method radiative transfer in multiple scattering and emitting layered media. *Appl. Optics* **27**, 2502–2509 (1988).

39. F. A.-M. Bender, H. Rodhe, R. J. Charlson, A. M. L. Ekman, N. Loeb, 22 views of the global albedo—Comparison between 20 GCMs and two satellites. *Tellus A* **58**, 320–330 (2006).

40. D. R. Feldman, C. A. Algieri, W. D. Collins, Y. L. Roberts, P. A. Pilewskie, Simulation studies for the detection of changes in broadband albedo and shortwave nadir reflectance spectra under a climate change scenario. *J. Geophys. Res.* **116**, D24103 (2011).

41. D. R. Feldman, C. A. Algieri, J. R. Ong, W. D. Collins, CLARREO shortwave observing system simulation experiments of the twenty-first century: Simulator design and implementation. *J. Geophys. Res.* **116**, D10107 (2011).

42. D. R. Feldman, W. D. Collins, J. L. Paige, Pan-spectral observing system simulation experiments of shortwave reflectance and longwave radiance for climate model evaluation. *Geosci. Model Dev.* **8**, 1943–1954 (2015).

43. B. A. Wielicki, D. F. Young, M. G. Mlynczak, K. J. Thome, S. Leroy, J. Corliss, J. G. Anderson, C. O. Ao, R. Bantges, F. Best, K. Bowman, H. Brindley, J. J. Butler, W. Collins, J. A. Dykema, D. R. Doelling, D. R. Feldman, N. Fox, X. Huang, R. Holz, Y. Huang, Z. Jin, D. Jennings, D. G. Johnson, K. Jucks, S. Kato, D. B. Kirk-Davidoff, R. Knuteson, G. Kopp, D. P. Kratz, X. Liu, C. Lukashin, A. J. Mannucci, N. Phojanamongkolkij, P. Pilewskie, V. Ramaswamy, H. Revercomb, J. Rice, Y. Roberts, C. M. Roithmayr, F. Rose, S. Sandford, E. L. Shirley, W. L. Smith, B. Soden, P. W. Speth, W. Sun, P. C. Taylor, D. Tobin, X. Xiong, Achieving climate change absolute accuracy in orbit. *Bull. Am. Meteorol. Soc.* **94**, 1519–1539 (2013).

44. Y. L. Roberts, P. Pilewskie, B. C. Kindel, D. R. Feldman, W. D. Collins, Quantitative comparison of the variability in observed and simulated shortwave reflectance. *Atmos. Chem. Phys* **13**, 3133–3147 (2013).

45. Y. L. Roberts, P. Pilewskie, D. R. Feldman, B. C. Kindel, W. D. Collins, Temporal variability of observed and simulated hyperspectral reflectance. *J. Geophys. Res. Atmos.* **119**, 10262–10280 (2014).

46. L. R. Brown, D. Chris Benner, J. P. Champion, V. M. Devi, L. Fejard, R. R. Gamache, T. Gabard, J. C. Hilico, B. Lavorel, M. Loete, G. C. Mellau, A. Nikitin, A. S. Pine, A. Predoi-Cross, C. P. Rinsland, O. Robert, R. L. Sams, M. A. H. Smith, S. A. Tashkun, V. G. Tyuterev, Methane line parameters in HITRAN. *J. Quant. Spectrosc. Radiat. Transf.* **82**, 219–238 (2003).

47. G. C. Toon, J.-F. Blavier, K. Sung, L. S. Rothman, I. E. Gordon, HITRAN spectroscopy evaluation using solar occultation FTIR spectra. *J. Quant. Spectrosc. Radiat. Transf.* **182**, 324–336 (2016).

48. M. J. Alvarado, V. H. Payne, K. E. Cady-Pereira, J. D. Hegarty, S. S. Kulawik, K. J. Wecht, J. R. Worden, J. V. Pittman, S. C. Wofsy, Impacts of updated spectroscopy on thermal infrared retrievals of methane evaluated with HIPPO data. *Atmos. Meas. Tech.* **8**, 965–985 (2015).

49. W. D. Collins, Parameterization of generalized cloud overlap for radiative calculations in general circulation models. *J. Atmos. Sci.* **58**, 3224–3242 (2001).

50. Y. Shuai, C. B. Schaaf, A. H. Strahler, J. Liu, Z. Jiao, Quality assessment of BRDF/albedo retrievals in MODIS operational system. *Geophys. Res. Lett.* **35**, L05407 (2008).

51. S. Y. Kotchenova, E. F. Vermote, R. Matarrese, F. J. Klemm Jr., Validation of a vector version of the 6S radiative transfer code for atmospheric correction of satellite data. Part I: Path radiance. *Appl. Optics* **45**, 6762–6774 (2006).

52. W. Lucht, C. B. Schaaf, A. H. Strahler, An algorithm for the retrieval of albedo from space using semiempirical BRDF models. *IEEE Trans. Geosci. Rem. Sens.* **38**, 977–998 (2000).

53. B. Briegleb, B. Light, "A Delta-Eddington Multiple Scattering Parameterization for Solar Radiation in the Sea Ice Component of the Community Climate System Model" (Technical Report NCAR/TN-472+STR, National Center for Atmospheric Research, 2007).

54. R. H. Moss, J. A. Edmonds, K. A. Hibbard, M. R. Manning, S. K. Rose, D. P. van Vuuren, T. R. Carter, S. Emori, M. Kainuma, T. Kram, G. A. Meehl, J. F. B. Mitchell, N. Nakicenovic, K. Riahi, S. J. Smith, R. J. Stouffer, A. M. Thomson, J. P. Weyant, T. J. Wilbanks, The next generation of scenarios for climate change research and assessment. *Nature* **463**, 747–756 (2010).

55. E. M. Volodin, N. A. Dianskii, A. V. Gusev, Simulating present-day climate with the INMCM4.0 coupled model of the atmospheric and oceanic general circulations. *Izv. Atmos. Ocean. Phy.* **46**, 414–431 (2010).

56. L. D. Rotstayn, S. J. Jeffrey, M. A. Collier, S. M. Dravitzki, A. C. Hirst, J. I. Syktus, K. K. Wong, Aerosol- and greenhouse gas-induced changes in summer rainfall and circulation in the Australasian region: A study using single-forcing climate simulations. *Atmos. Chem. Phys.* **12**, 6377–6404 (2012).

57. K. E. Taylor, V. Balaji, S. Hankin, M. Juckes, B. Lawrence, S. Pascoe, CMIP5 data reference syntax (DRS) and controlled vocabularies, Version 1.2 (2011).

58. T. Andrews, J. M. Gregory, M. J. Webb, K. E. Taylor, Forcing, feedbacks and climate sensitivity in CMIP5 coupled atmosphere-ocean climate models. *Geophys. Res. Lett.* **39**, L09712 (2012).

59. W. D. Collins, P. J. Rasch, B. A. Boville, J. J. Hack, J. R. McCaa, D. L. Williamson, J. T. Kiehl, B. Briegleb, "Description of the NCAR Community Atmosphere Model (CAM3.0)" (Technical Report NCAR/TN-464+STR, National Center for Atmospheric Research, 2004).

60. W. D. Collins, P. J. Rasch, B. A. Boville, J. J. Hack, J. R. McCaa, D. L. Williamson, B. P. Briegleb, C. M. Bitz, S.-J. Lin, M. Zhang, The formulation and atmospheric simulation of the community atmosphere model version 3 (CAM3). *J. Climate* **19**, 2144 (2006).

Citation: W. D. Collins, D. R. Feldman, C. Kuo, N. H. Nguyen, Large regional shortwave forcing by anthropogenic methane informed by Jovian observations. *Sci. Adv.* **4**, eaas9593 (2018).

Science Advances

Large regional shortwave forcing by anthropogenic methane informed by Jovian observations

William D. Collins, Daniel R. Feldman, Chaincy Kuo and Newton H. Nguyen

ARTICLE TOOLS	http://advances.sciencemag.org/content/4/9/eaas9593
SUPPLEMENTARY MATERIALS	http://advances.sciencemag.org/content/suppl/2018/09/24/4.9.eaas9593.DC1
REFERENCES	This article cites 49 articles, 1 of which you can access for free http://advances.sciencemag.org/content/4/9/eaas9593#BIBL
PERMISSIONS	http://www.sciencemag.org/help/reprints-and-permissions

Use of this article is subject to the Terms of Service